Determining the boundary of dynamical chaos in the generalized Chirikov map via machine learning

Daniil Chernyshov, Arkady Satanin, and Lev Shchur

HSE University, 101000 Moscow, Russia

We investigate the boundary separating regular and chaotic dynamics in the generalized Chirikov map, an extension of the standard map with phase-shifted secondary kicks. Lyapunov maps were computed across the parameter space (K, K_α, τ) and used to train a convolutional neural network (ResNet18) for binary classification of dynamical regimes. The model reproduces the known critical parameter for the onset of global chaos in the standard map and identifies two-dimensional boundaries in the generalized map for varying phase shifts τ. The results reveal systematic deformation of the boundary as τ increases, highlighting the sensitivity of the system to phase modulation and demonstrating the ability of machine learning to extract interpretable features of complex Hamiltonian dynamics. This framework allows precise characterization of stability boundaries in nontrivial nonlinear systems.

Introduction. — Many fundamental problems in physics reduce to the study of Hamiltonian systems with two degrees of freedom. Examples include the restricted three-body problem, the motion of atomic chains in a periodic potential (the Frenkel–Kontorova model), the description of particle orbits in accelerators, and the acceleration of cosmic particles (Fermi acceleration) [1]. At the same time, the equations governing the dynamics of nonlinear systems are, in the most interesting cases, typically non-integrable. According to H. Poincaré, non-integrability arises from the presence of unstable hyperbolic points in phase space, which gives rise to homoclinic structures of trajectories near the separatrix [2, 3]. In dynamical systems, variations of parameters may lead to resonance capture (both primary and secondary), the formation of stochastic layers around the separatrix, resonance overlap, and ultimately the onset of global chaos [4, 5]. The scenario outlined above is rather general; however, for practically relevant systems, fundamental questions remain unanswered: *Does a boundary exist between chaos and order in phase space? What is the structure of the fractal geometry of stochastic regions?*

For systems with 3/2 degrees of freedom, the qualitative scenario of chaos development, following the description of B.V. Chirikov [4, 5], can be outlined as follows. As the amplitude of the external periodic force increases, the system first undergoes resonance capture. Owing to periodicity, chains of resonances then appear, around which closed invariant curves are formed. A further increase of the perturbation results in the separatrix becoming embedded in a stochastic layer, eventually leading to resonance overlap. As the amplitude increases, a "stochastic sea" forms in phase space (in the Poincaré map), within which small islands of regular motion are embedded. Chirikov's resonance-overlap scenario provides insight into the mechanism underlying the formation of the global structure of chaos; however, the arguments presented are not rigorous and are largely based on numerical experiments. The most accurate value of the control parameter for the Chirikov map was determined in [6]. Further accounts of recent advances in the theory of dynamical chaos in two-dimensional systems can be found in [7–10] and the references therein.

In this work, we focus on the properties of the boundary between regular and stochastic motion, using the standard map — the Chirikov map — as an example. It is well known that in the case of the Chirikov map, resonance overlap appears only at the second order of perturbation theory (the overlap of "virtual resonances"). We consider a generalized Chirikov map, which represents a natural extension of the standard map through the introduction of phase-shift parameters and an additional external forcing ("binary signal"). This modification leads to a more complex structure of phase-space regions already at the leading order, allowing the inclusion of additional control mechanisms for chaos management and opening new possibilities for identifying the boundary between regular and chaotic dynamics in nontrivial cases. As noted by Chirikov [5], even a single trajectory of a nonlinear dynamical system carries a wealth of information about the system, making the processing of numerical data a significant challenge. Importantly, in the Chirikov map, the system trajectory between successive perturbations is known exactly, ensuring numerical stability of the iteration procedure. The map considered in this work preserves this property, allowing the generation of long trajectories.

Recent progress in addressing various problems in the theory of dynamical systems has been driven by advances in modern supercomputing and quantum computation technologies, as well as the application of neuromorphic methods for data processing and analysis. As an example of using recognition, classification, and large-scale data analysis methods in the study of phase transitions and critical phenomena, see [11, 12]. In the present work, we propose to employ machine learning techniques to determine the stability boundary of a system, in other words, to identify the boundary between chaos and order.

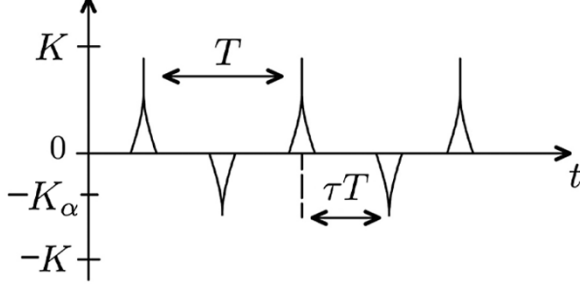To determine the stability boundary in the generalized

FIG. 1. Binary sequence of kicks. Vertical axis: dimensionless amplitude of the primary kicks, K, applied at times nT; K_α denotes the amplitude of the secondary kicks applied at times $nT + \tau T$ (phase shift τT).

Chirikov map, modern methods of data analysis using machine learning will be employed. First, training and validation datasets will be generated in the form of Lyapunov maps corresponding to various parameters of the standard map. Next, a suitable neural network architecture will be selected. This will be followed by data preparation for training the neural network and the network training itself. Based on these calculations, a binary classification of Lyapunov maps of the generalized Chirikov map will be performed using the trained neural network.

Based on the conducted analysis, and also drawing on Greene's theory [6] in the extended parameter space, the boundary between chaos and order will be described.

Generalized Chirikov map. — The Hamiltonian of a planar rotator subjected to a "binary" sequence of kicks, schematically illustrated in Figure 1, can be written as:

$$H = \frac{I^2}{2} + \cos\theta \left[K \sum_{n=-\infty}^{\infty} \delta(t - nT) \right.$$

$$\left. - K_\alpha \sum_{n=-\infty}^{\infty} \delta(t - T(n+\tau)) \right], \quad (1)$$

where (I, θ) denote the generalized momentum of the rotator with unit moment of inertia and the generalized coordinate (angle), respectively; K and K_α are the constants characterizing the action of the external force on the rotator; T is the period of the external force; and τT is the phase shift.

Since no external force acts on the rotator between kicks, the generalized momentum remains constant, while the phase evolves with a uniform angular velocity. This allows one to directly write down the generalized map for the corresponding pairs of variables. Let $I_n \equiv I(nT)$ and $\theta_n \equiv \theta(nT)$ be defined immediately before the kick applied at time nT. Under the action of the "positive" kick at nT, the momentum changes according to $I_{n+\tau} =$ $I_n + K\sin\theta_n$, after which the phase evolves freely and, over the time interval τT, acquires an increment of $\tau I_{n+\tau}$ (with $I_{n+\tau} \equiv I(nT + \tau T)$ and $\theta_{n+\tau} \equiv \theta(nT + \tau T)$). A similar update of the action variable and phase occurs under the "negative" kick at $(n + \tau)T$. Consequently, after one period, the combined map takes the form:

$$\begin{cases} I_{n+\tau} = I_n + K\sin\theta_n, \\ \theta_{n+\tau} = \theta_n + \tau I_{n+\tau}, \end{cases}$$

$$\begin{cases} I_{n+1} = I_{n+\tau} - K_\alpha \sin\theta_{n+\tau}, \\ \theta_{n+1} = \theta_{n+\tau} + (1-\tau)I_{n+\tau}. \end{cases}$$

It should be noted that we have rescaled the variables as follows: $I_n T \to I_n$, $KT \to K$, $K_\alpha T \to K_\alpha$.

By eliminating the intermediate variables $I_{n+\tau}$ and $\theta_{n+\tau}$, we obtain:

$$\begin{cases} I_{n+1} = I_n + K\sin\theta_n \\ \qquad - K_\alpha \sin\bigl(\theta_n + \tau(I_n + K\sin\theta_n)\bigr), \\ \theta_{n+1} = \theta_n + \tau(I_n + K\sin\theta_n) + (1-\tau)I_{n+1}. \end{cases} \quad (2)$$

It is evident that for $K_\alpha = 0$, the map (2) reduces to the Chirikov map, while in the case $K = 0$ and $K_\alpha \neq 0$, the map again (after the phase shift) reduces to the Chirikov map.

Note that, due to the periodicity of the $\sin\theta$ function, the system dynamics can be conveniently considered on a torus by taking $[(I, \theta) \bmod 2\pi]$. Mathematically, the standard map is a two-dimensional Hamiltonian (symplectic) map that preserves phase-space volume, i.e., its Jacobian is equal to 1 at every point in the phase space.

Let us first discuss the case $K_\alpha = 0$. As the coupling constant K increases, the resonances overlap and are destroyed according to the scenario developed by Chirikov [4, 5], after which secondary resonances emerge within the stochastic sea. The value of K at which the invariant torus is destroyed and global chaos appears has been determined by various authors. Greene's method is the most precise of those developed to date, yielding $K_c \approx 0.971635406$ [6].

To further quantify the system's dynamics and the onset of chaos, we analyze the Lyapunov exponents, which measure the rate of exponential divergence of trajectories in phase space. A trajectory on the torus is generated by choosing an initial point with coordinates (I_0, θ_0). Iterating the map (2) N times yields the trajectory $(I_0, \theta_0), \ldots, (I_n, \theta_n), \ldots, (I_N, \theta_N)$. If the initial conditions are slightly perturbed, the trajectory changes to $(I_n + \delta I_n, \theta_n + \delta\theta_n)$. The maximal Lyapunov exponent is defined as $\Lambda = \lim_{N\to\infty} \Lambda_N$, where

$$\Lambda_N = \frac{1}{N} \sum_{n=1}^{N} \ln\frac{d_n}{d_{n-1}}.$$

where $d_n = \sqrt{\delta I_n^2 + \delta\theta_n^2}$, with d_0 being the initial distance between nearby points in phase space. The infinitesimal deviations are obtained by jointly solving (2) and

$$
\begin{cases}
\delta I_{n+1} = \left(1 - \tau K_\alpha \cos(\theta_n + \tau(I_n + K\sin\theta_n))\right)\delta I_n \\
\qquad + \Big[K\cos\theta_n - K_\alpha\cos(\theta_n + \tau(I_n + K\sin\theta_n)) \\
\qquad \times (1 + \tau K\cos\theta_n)\Big]\delta\theta_n, \\
\delta\theta_{n+1} = \left(1 + \tau K\cos\theta_n\right)\delta\theta_n \\
\qquad + \tau\delta I_n + (1-\tau)\delta I_{n+1}.
\end{cases}
\tag{3}
$$

The system (3) allows us to investigate the stability of fixed points of the map (2). For example, in the case $K_\alpha = 0$, the stationary point $(0, \pi)$ is found to be a stable elliptic point for $0 \le K \le 4$. For $K \ge 4$, the stationary point $(0, \pi)$ loses stability and becomes hyperbolic. Similarly, the fixed point $(0, \pi)$, which is elliptic when $K_\alpha = 0$, turns into an unstable hyperbolic point for $K = 0$ and $K_\alpha \ne 0$. Interestingly, when $K = K_\alpha$, the map (2) exhibits fixed points that depend on the phase τ, while the point $(0, \pi)$ remains stable for any value of τ.

In conclusion of this section, we note that a detailed study of the fine structure of the phase portrait generated by the Chirikov map, which exhibits fractal properties, remains an open problem to date.

Data generation. — The generalized Chirikov map (2) exhibits both regular and chaotic behavior depending on the parameters K, K_α, τ. To classify the dynamical regimes based on the maximal Lyapunov exponent in the phase space $(I, \theta) \in [0, 2\pi]^2$, machine learning methods are employed. This approach allows formalizing the problem of identifying the nature of a trajectory as a binary image classification task [13, 14].

For training and validation of the neural network, a dataset of Lyapunov maps with a resolution of 64×64 pixels was generated. Each image corresponds to a phase portrait in which the horizontal axis represents the variable $\theta \in [0, 2\pi]$, the vertical axis represents $I \in [0, 2\pi]$, and the color of each point encodes the value of the maximal Lyapunov exponent at the corresponding location in phase space: "warmer" colors indicate larger exponent values, whereas "cooler" colors correspond to smaller ones.

Using numerical simulations of the standard map and subsequent computation of Lyapunov exponents [15], a dataset of 400 Lyapunov maps was generated, comprising 200 maps corresponding to regular dynamics ($K < K_c$) and 200 maps corresponding to chaotic dynamics ($K > K_c$). To enhance symmetry learning in the model, in each regime 100 images were generated using the standard map ($K \ne 0$, $K_\alpha = 0$) and 100 images using the generalized Chirikov map with parameters equivalent to those of the standard map ($K = 0$, $K_\alpha \ne 0$).
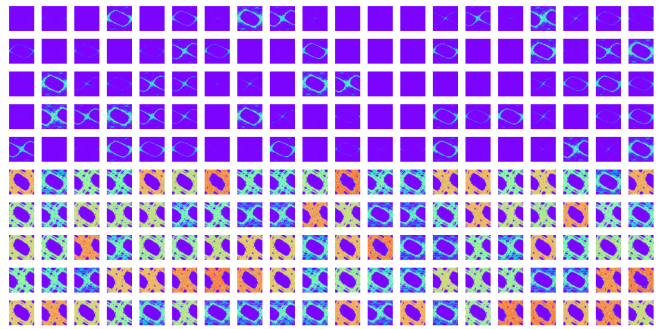

FIG. 2. Example of Lyapunov maps used for training and validation of the neural network. The top five rows correspond to regular dynamics, while the bottom rows correspond to chaotic dynamics.

Within each regime, the control parameters were sampled uniformly. For the standard map, $K \sim \mathcal{U}(\delta, K_c - \varepsilon)$ for regular dynamics and $K \sim \mathcal{U}(K_c, 1.5)$ for chaotic dynamics; for the generalized Chirikov map, K_α was sampled analogously, $K_\alpha \sim \mathcal{U}(\delta, K_c - \varepsilon)$ for regular dynamics and $K_\alpha \sim \mathcal{U}(K_c, 1.5)$ for chaotic dynamics, with $0 < \delta \ll 1$. Each image was assigned a binary label: 0 for regular dynamics and 1 for chaotic dynamics. Examples of the generated images are shown in Figure 2.

Model. — To address the binary classification task of Lyapunov maps, a convolutional neural network [16] based on ResNet18 [17] was employed and adapted to the specific requirements of the problem. In particular, the first convolutional layer was modified to accommodate the small input size (64×64), and the initial max-pooling operation was removed to preserve feature resolution in the early layers. The final fully connected layer was replaced by a two-output layer corresponding to the classes "regular" and "chaotic" dynamics.

The choice of the ResNet architecture is supported by several studies linking it to numerical methods for solving differential equations and the analysis of dynamical systems. In [18], it was shown that residual blocks can be interpreted as a time discretization of evolutionary partial differential equations, providing a rigorous mathematical connection between the network depth and the integration steps of the dynamical system. In [19], it was demonstrated that ResNet is capable of reproducing trajectories of ordinary differential equations and predicting their evolution stably over horizons much longer than the training data. Furthermore, [20] proposed a multilevel approach to modeling spatiotemporal dynamics, where ResNet blocks are used to preserve the structure of the corresponding differential equations, enabling efficient representation of complex spatiotemporal processes. These findings indicate that the ResNet architecture not only achieves high performance in traditional computer vision tasks but also has significant potential for modeling and analyzing complex dynamical systems.
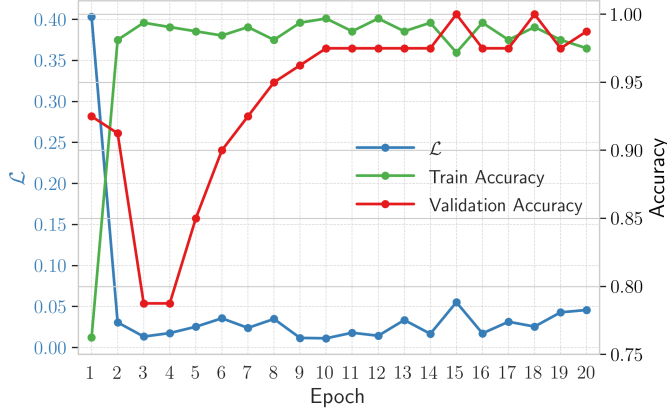
FIG. 3. Training dynamics of the neural network. Left vertical axis: loss function $\mathcal{L}$; right vertical axis: Accuracy. Horizontal axis: epoch number
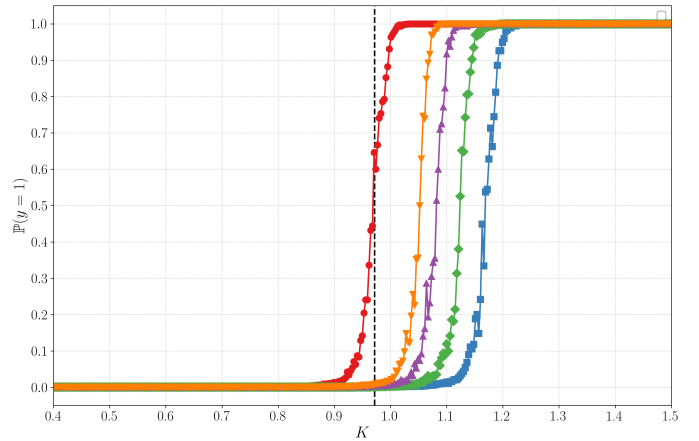

FIG. 4. Probability of classifying the Lyapunov map as chaotic, $\mathbb{P}(y = 1)$, predicted by the neural network as a function of the parameter K in the generalized Chirikov map. Colored curves (from left to right) correspond to the parameter sets ($K_\alpha = 0$, $\tau = 0$), ($K_\alpha = 0.2$, $\tau = 0.5$), ($K_\alpha = 0.2$, $\tau = 0.25$), ($K_\alpha = 0.2$, $\tau = 0.1$), and ($K_\alpha = 0.2$, $\tau = 0$). The vertical dashed line indicates the critical value K_c.

Data preprocessing and training. — Prior to training, standard data augmentation techniques were applied to the Lyapunov map images to improve the generalization capability of the neural network. Specifically, random horizontal and vertical flips, as well as rotations up to 20°, were performed.

Following these augmentations, the full dataset of 400 images was uniformly shuffled to preserve class balance and then split into training and validation sets with an 80:20 ratio. The model was trained using the Adam optimizer [21] with parameters $\alpha = 10^{-3}$, $\beta_1 = 0.9$, $\beta_2 = 0.999$, $\varepsilon = 10^{-8}$, and weight decay $\lambda = 10^{-4}$, in combination with a cosine annealing learning rate schedule with $T_{\max} = 10$. Binary cross-entropy was used as the loss function, and the network was trained for 20 epochs.

Figure 3 shows the values of the loss function $\mathcal{L}$ on the training set, as well as the classification accuracy on the training $\text{Accuracy}_{\text{train}}$ and validation $\text{Accuracy}_{\text{val}}$ sets. The classification accuracy is defined as:

$$\text{Accuracy} = \frac{TP + TN}{TP + TN + FP + FN},$$

where TP denotes the number of true positive predictions, TN the number of true negatives, FP the number of false positives, and FN the number of false negatives.

It can be observed that the loss $\mathcal{L}$ reaches its minimum at the 10th epoch, while the maximum classification accuracy $\text{Accuracy}_{\text{val}}$ is attained at the 15th epoch. This indicates that the neural network has effectively learned to distinguish between regular and chaotic dynamics in the standard map.

Results analysis. — Further analysis allows us to assess the sensitivity of the trained model to variations in the parameter K. Figure 4 shows the dependence of the probability of classifying a Lyapunov map as chaotic on the value of the parameter K in the generalized Chirikov

map.

The obtained results are in good agreement with the established theory. For $K_\alpha = 0$ and $\tau = 0$ (red curve), the transition from regular to chaotic dynamics occurs near the critical value $K_c \approx 0.97$. Following Greene's argument [6], this threshold for the Chirikov standard map is defined by the value of the coupling parameter K at which the last invariant curve on the two-dimensional torus is destroyed. In the generalized Chirikov map, two additional parameters, K_α and τ, influence the dynamics. When $\tau = 0$, the dependence of the critical boundary on K_α (Figure 4) can be attributed to the effective reduction of the coupling constant in the Hamiltonian (1), which delays the destruction of the invariant curve. When $\tau \neq 0$, the introduction of a second series of δ-functions explicitly depends on τ, making the shape of the critical boundary phase-dependent. For instance, for $K_\alpha = 0.2$ and $\tau = 0$, the transition boundary shifts to the right along the K-axis, as the additional kicks compensate the primary ones by the amount K_α. This effect is demonstrated by the blue curve.

It is of particular interest to examine the response of the neural network to the introduction of the parameter τ, which modulates the phase of the additional sequence of kicks in (2).

Figure 5 shows the predictions $\hat{y}$ obtained on a uniform grid in the (K, K_α) parameter plane for different values of τ. These results were obtained by computing Lyapunov maps of the generalized Chirikov map, which were then provided as input to the neural network to classify the corresponding dynamical regime. Predictions for cases with $\tau > 0$ were obtained in the same manner.
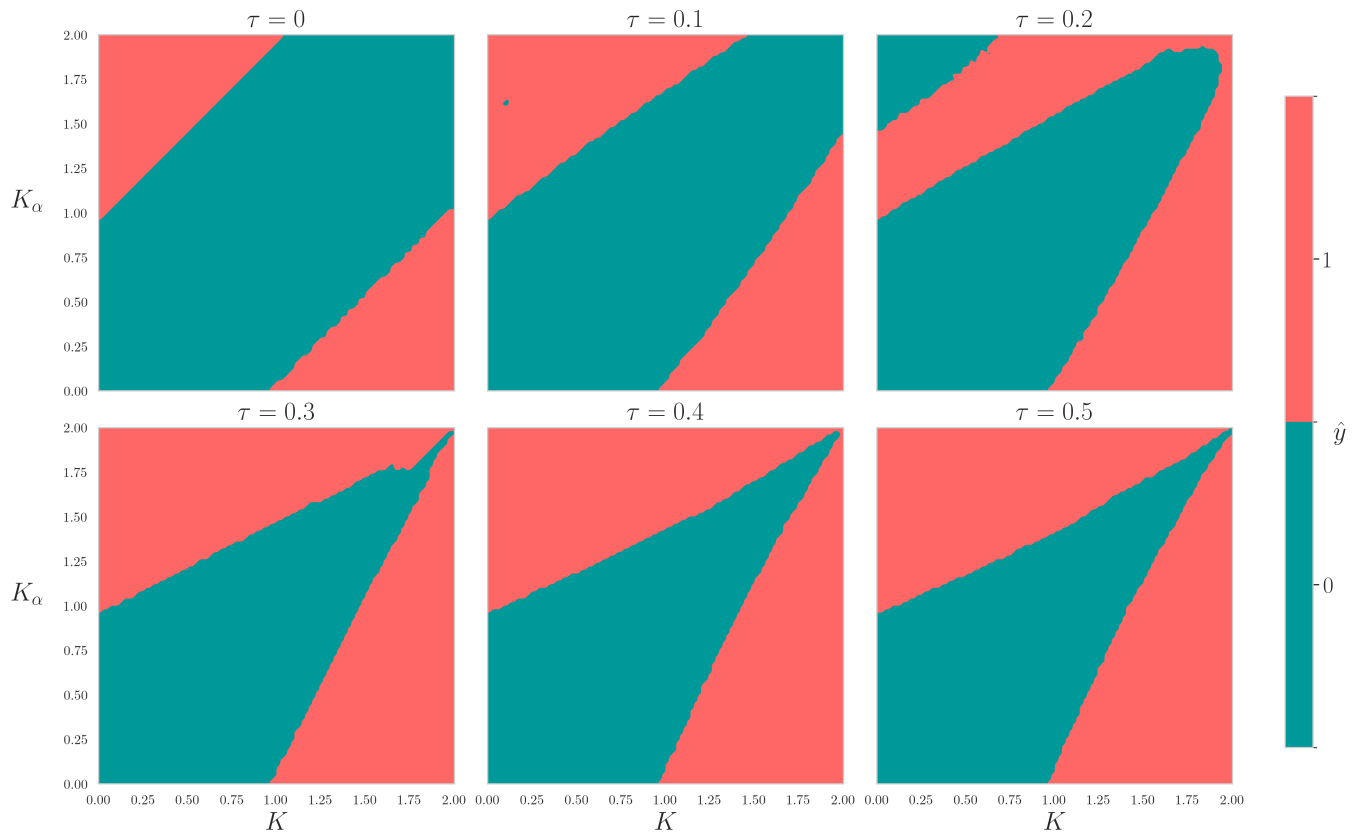
Although isolated classification errors are present, the

FIG. 5. Neural network predictions $\hat{y}$ on a uniform 100×100 grid in the (K, K_α) parameter plane for $\tau = 0, 0.1, 0.2, 0.3, 0.4, 0.5$. Green: regular regime ($\hat{y} = 0$); red: chaotic regime ($\hat{y} = 1$).

model successfully captures the overall distinction between dynamical regimes. In particular, the predictions exhibit a clear symmetry with respect to the parameter exchange $(K, K_\alpha) \mapsto (K_\alpha, K)$, which reflects the partial compensation of the δ-kicks in (2).

As τ increases, this symmetry gradually deteriorates: the upper corners of the chaotic domains approach one another, forming a wedge-like structure. While for $\tau = 0$ the boundary between regular and chaotic regions is approximately linear and can be expressed as $K_\alpha \approx aK + b$, for $\tau > 0$ it takes the more general form $K_\alpha \approx f(K, \tau)$, where f is a smooth function capturing the effect of the phase shift. This observation highlights the sensitivity of the system's behavior to the phase parameter τ while preserving the interpretability of the model's predictions.

Discussion. — In summary, the proposed methodology for data generation and analysis in the context of the generalized Chirikov map has enabled the identification of new features of the stability boundary using machine learning techniques. The analysis demonstrated that the neural network successfully reproduces known results regarding the critical parameter for the onset of global chaos in the standard map. In the case of the generalized Chirikov map, the network exhibits satisfactory classification performance for different types of dynam-

ics, including the existence of two-dimensional boundaries separating regular and chaotic regions, the behavior of boundary curves in agreement with Greene's theory [6], and the prediction of unusual phase dependencies of mixed signals. As the number of control parameters increases, certain difficulties arise, associated with incorrect classification of specific system configurations, indicating the need for further improvement in the model's robustness.

[1] A.J. Lichtenberg and M.A. Lieberman, *Regular and Stochastic Motion*, vol. 38, Springer Science & Business Media, 2013.

[2] H. Poincaré, *New Methods of Celestial Mechanics*, nos. 450-451, National Aeronautics and Space Administration, 1967.

[3] V.V. Kozlov, *Integrability and Non-Integrability in Hamiltonian Mechanics*, Russian Mathematical Surveys **38**(1), 1–76 (1983).

[4] B.V. Chirikov, *Research Concerning the Theory of Non-Linear Resonance and Stochasticity*, CM-P00100691, CERN-Trans-71-40, 1971.

[5] B.V. Chirikov, *A Universal Instability of Many-Dimensional Oscillator Systems*, Physics Reports **52**(5), 263–379 (1979).

[6] J.M. Greene, *A Method for Determining a Stochastic Transition*, Journal of Mathematical Physics **20**(6), 1183–1201 (1979).

[7] G.M. Zaslavsky, *Hamiltonian Chaos and Fractional Dynamics*, Oxford University Press, 2005.

[8] L.E. Reichl, *Transition to Chaos*, Springer International Publishing, 2021.

[9] M. Mugnaine, B.B. Leal, I.L. Caldas, A.M.O. de Almeida, and R.L. Viana, *Isochronous Bifurcations in a Two-Parameter Twist Map*, Phys. Rev. E **110**(2), 024206 (2024).

[10] I.I. Shevchenko, *Dynamical Entropy of the Separatrix Map*, Phys. Rev. E **111**(3), 034211 (2025).

[11] J. Carrasquilla and R.G. Melko, *Machine Learning Phases of Matter*, Nat. Phys. **13**(5), 431–434 (2017).

[12] V. Chertenkov, E. Burovski, and L. Shchur, *Finite-Size Analysis in Neural Network Classification of Critical Phenomena*, Phys. Rev. E **108**(3), L032102 (2023).

[13] I. Goodfellow, Y. Bengio, and A. Courville, *Deep Learning*, vol. 1, 2nd ed., MIT Press, Cambridge, 2016.

[14] A. Krizhevsky, I. Sutskever, and G.E. Hinton, *ImageNet Classification with Deep Convolutional Neural Networks*, Advances in Neural Information Processing Systems **25**, 2012.

[15] G. Benettin, L. Galgani, A. Giorgilli, and J.-M. Strelcyn, *Lyapunov Characteristic Exponents for Smooth Dynamical Systems and for Hamiltonian Systems; A Method for Computing All of Them. Part 1: Theory*, Meccanica **15**(1), 9–20 (1980).

[16] K. O'Shea and R. Nash, *An Introduction to Convolutional Neural Networks*, arXiv:1511.08458 (2015).

[17] K. He, X. Zhang, S. Ren, and J. Sun, *Deep Residual Learning for Image Recognition*, in: Proceedings of the IEEE Conference on Computer Vision and Pattern Recognition, pp. 770–778, 2016.

[18] L. Ruthotto and E. Haber, *Deep Neural Networks Motivated by Partial Differential Equations*, Journal of Mathematical Imaging and Vision **62**(3), 352–364 (2020).

[19] A. Chashchin, M. Botchev, I. Oseledets, and G. Ovchinnikov, *Predicting Dynamical System Evolution with Residual Neural Networks*, arXiv:1910.05233 (2019).

[20] X.-Y. Liu, M. Zhu, L. Lu, H. Sun, and J.-X. Wang, *Multi-Resolution Partial Differential Equations Preserved Learning Framework for Spatiotemporal Dynamics*, Communications Physics **7**(1), 31 (2024).

[21] D.P. Kingma and J. Ba, *Adam: A Method for Stochastic Optimization*, arXiv:1412.6980 (2014).